Correlation between Ball Milling Parameters and Microstructure Parameters of Nanocopper Using XRD Method

O. BOYTSOV[4], F. BERNARD[1], E. GAFFET[2], Y. CHAMPION[3] and A. USTINOV[4]

[1]*LRRS UMR 5613 CNRS/Université de Bourgogne – BP 47870 21078 DIJON Cedex (France)*

E-mail: fbernard@u-bourgogne.fr

[2]*Nanomaterials Research Group UMR 5060 CNRS/UTBM – 90010 Belfor (France)*

E-mail: eric.gaffet@utbm.fr

[3]*CECM – CNRS, 15 rue Georges Urbain, 94407 Vitry-sur-Seine (France)*

E-mail: yannick.champion@glvt-cnrs.fr

[4]*Institute for Metal Physics, Pr. Vernadskogo, 36, Kiev 03142 (Ukraine)*

E-mail: ustinov@paton-icebt.kiev.ua

Abstract

The microstructure evolution of Cu-nanostructured powders *versus* the ball milling conditions was investigated using X-ray diffraction analysis. The characteristics of as-milled Cu powder microstructure in terms of crystallite size, dislocations and twin boundary densities were determined by fitting the simulated X-ray diffraction peak profiles to the experimental ones in order to establish a correlation between the powder microstructure and the ball milling parameters. It was shown that the simulated X-ray diffraction peak profiles agree satisfactorily with the experimental ones taking into account transmission electronic microscopy observations where twin boundaries and dislocations were observed.

INTRODUCTION

In spite of a lot of research effort, the mechanism of phase formation during ball milling (MA) is not well understood. It is most often proposed that the process of MA introduces a variety of defects (vacancies, dislocations, grain boundaries, stacking faults, *etc.*) which raise the free energy of the system making it possible to produce metastable phases. But there are very few investigations that deal with the characterization and the quantification of the defects produced in mechanically alloyed powders. As a primary investigation, the effect of the mechanical activation mode (*i.e.* the friction or direct shock ones, at least the component ratio of both components) can be assumed on analyzing the microstructure of post-mortem milled powders. X-ray diffraction (XRD) is really a valuable technique for characterization in terms of material microstructure. Indeed, the ball milling of metals or alloys induces extended variations in the intensity distribution of XRD diagrams and, in particular, in the line profile.

An influence of major planar defects, namely, stacking and twin faults, on the X-ray diffraction of crystal was studied theoretically and reported in numerous papers [1]. Indeed, according to Warren [2], the shift, the broadening and the asymmetry parameters of the component profile are proportional to the fault densities and significantly depend on the (*hkl*) indices of the component reflections. Several authors reported on the experimental evidence of the influence of stacking and twin faults on XRD profiles [2–8]. Recent investigations have shown that the conventional XRD line profile analysis methods (*i.e.* Williamson–Hall [9] and Warren–Averbach methods [10] must be updated, in order to take into account

TABLE 1

Ball milling conditions [Ω (r.p.m.)/ω (r.p.m.)/Δ*t* (h)] and ball milling characteristics determined from ref. [13]

Conditions	Power, W/ball	Frequency, Hz	Energy, J
150 /50 /24 h	0.18	6	0.03
250 /50 /24 h	0.79	9	0.08
350 /50 /24 h	2.1	12.7	0.16

the contrast effect of dislocations or planar defects on the peak broadening.

A new whole pattern fitting procedure is proposed. It takes into account the dependence of the crystallite size, of the residual strains as well as of the planar defects, on the XRD peak broadening that may be observed on ball milled materials. Such a method will allow one to understand the influence of ball milling parameters for controlling the synthesis of nanostructured materials. The work concerns the XRD modeling, in a kinematic approach, of *fcc* nanocopper produced by ball milling and containing a high concentration of structural defects.

PREPARATION AND CHARACTERIZATION OF MILLED POWDERS

Pure elemental copper powders were milled with a planetary mill referred to as G5 milling machine [11–13]. 125 ml of powders and 5 stainless steel balls (15 mm in diameter, 14 g in mass) were sealed under air, into the stainless steel vials. The ball to powder mass ratio is 7/1. The rotation speed of its vials (ω, anticlockwise rotation) which are fixed onto a rotating disk and the rotation speed of disk (Ω, clockwise rotation) can be set independently. Each milling condition is characterized by 3 essential parameters (Ω (rpm)/ω (rpm), Δ*t* (h)) where Δ*t* is the duration of the milling process. The XRD patterns of powders produced under conditions 150/50/24, 250/50/24 and 350/50/24 corresponding to three different power values of shocks were selected to test the performance of our model (Table 1) when the energy of shocks is mainly favoured (*i.e.* when the direct shock mode is promoted, Ω > ω, see details in [12]). XRD analyses were performed with a

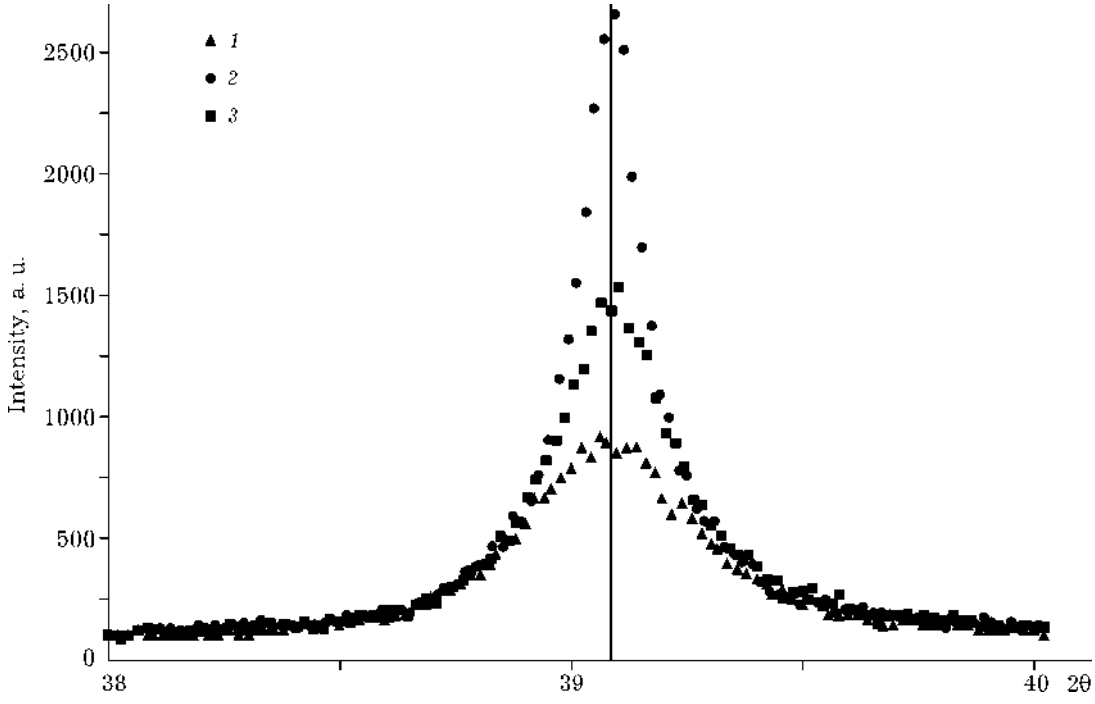

Fig. 1. Fragments of experimentally (111) XRD patterns of Cu-powders which have been milled under different conditions: *1* – 150/50/24 h, *2* – 250/50/24 h, *3* – 350/50/24 h.

D5000 Siemens high resolution diffractometer using a monochromatic CuK_β beam ($\lambda = 0.1392$ nm) obtained by a curved graphite monochromator in the diffracted beam. The morphology and size of the crystallites (shape and size of the coherently diffracting domains) and the structural imperfections (microstrains, stacking faults, *etc.*) in the as-milled powders were determined using the XRD profile analysis described by Langford and Louër [14].

Figure 1 shows fragments of (111) XRD peaks experimentally obtained for each ball milling condition. From these profiles which are modelled by the symmetric pseudo-Voigt function, an anomalous angular dependence of the integral breadth was observed. Indeed, a standard Williamson–Hall plot presented Fig. 2 in the case of 250/50/24 h milling condition, has been found to exhibit a non-monotonous change of the integral breadths $\beta^* = \beta\cos(\theta/\lambda)$ *vs.* $d^* = 2\sin(\theta/\lambda)$ where β is the integral breadth, q is the angle peak position and λ is the X-ray wavelength. Despite anisotropic effect, the linear regression on Williamson–Hall data (based on least squares method) brings an evaluation of the apparent size and the microdistortions for these Cu crystallites, respectively equal to 42 nm and 0.0016 for a such milling condition.

However, the average particle diameter was estimated as being about 50 to 200 μm, from BET specific surface measurements and assuming a spherical shape. The large difference between particle size and crystallite size (20–120 nm from Williamson–Hall plot), is easily explained by the combined effect of fracture, agglomeration and consolidation processes that materials undergo during the severe mechanical treatment. Besides, aggregate formation induced by the ball milling process was confirmed by scanning electron microscopy observations (Fig. 3). The mechanically activated powders may be considered as aggregates composed of Cu-nanocrystallites (40–100 nm) as confirmed by SEM observation in Fig. 3, *b*.

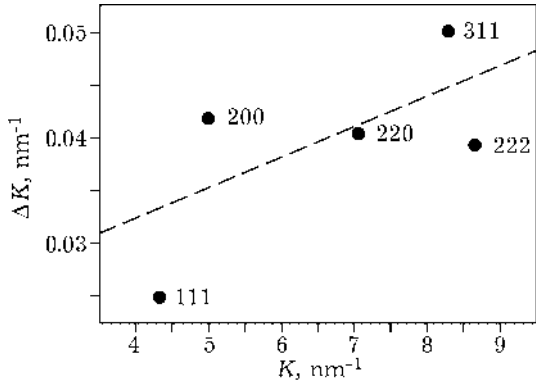

Fig. 2. Standard Williamson–Hall plot for a copper powder prepared in the case of 150/50/24 h ball milling condition.

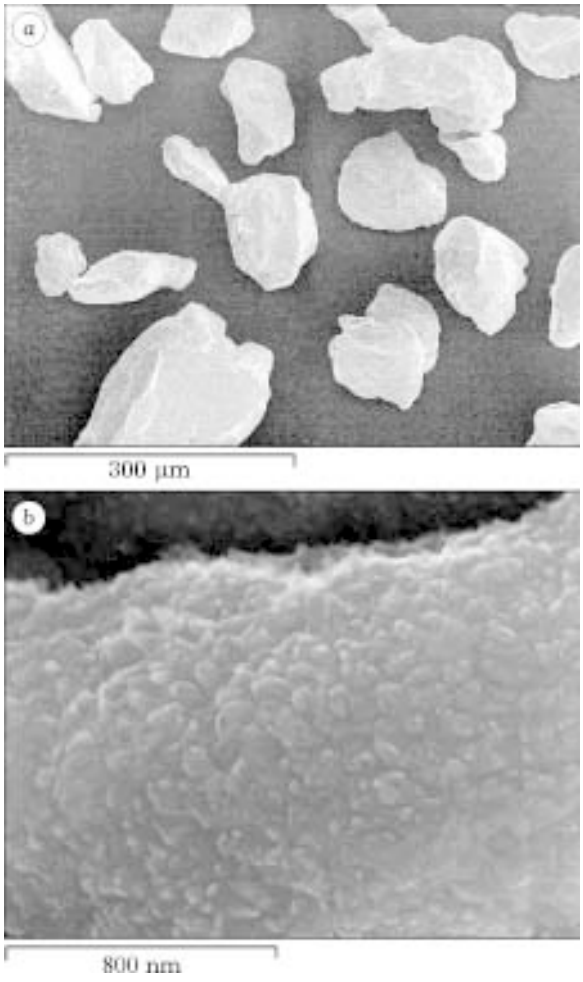

Fig. 3. SEM photographs of Cu-milled powders according to 150/50/24 h ball milling condition: *a* – view of Cu aggregates (×200); *b* – view of the surface of one aggregate (×70 000).

Transmission electron microscopy was carried out using a TOPCON 002B microscope (working at 200 kV, with a point resolution of 0.18 nm) on the powders as-deposited on a carbon grid. The possible contamination by milling media and tools was evaluated by EDX analyses on pressed pellets. Analysis shows slight pollution by chromium and iron, never exceeding 1 at. %. Consequently, the effect of these impurities was not taken into account in

this paper. Indeed, no cell parameter evolution of Cu was observed.

MODELING PROCEDURE

Usually, broadening of XRD peaks is known to depend on the size of coherently diffracting domains and the mean value of microdistortions of the crystal lattice, but also on the presence of dislocations and stacking faults as well. According to [15], let us consider that each microstructure characteristic gets a value which does not depend on the value of other characteristics, all components of XRD peaks can be calculated as a convolution of functions describing XRD peak profile changes caused by stacking faults, the finite size of the coherently diffracting domains (size factor), of dislocations and their distributions in the crystal and elastic properties of the crystal (microdistortion factor).

Thus, considering all the data discussed in [15], the XRD intensity may be expressed as follows:

$$I(\vartheta)=\Sigma I_s(H_s^\theta K_s^\theta L_i^\theta)\otimes S_s(\vartheta)\otimes D(\vartheta)\otimes A(\vartheta) \quad (1)$$

where $I_s(H_s^\theta K_s^\theta L_i^\theta)$ is the intensity of the *s*-component of a peak scattered at ϑ angle by a crystal with planar defects; $\otimes$ means a convolution procedure. The detailed description of each function is published elsewhere [15]. For the given $H_s^\theta K_s^\theta L_i^\theta$ coordinates, the scattered intensity at the angle ϑ can be determined as follows:

$$I_p(\vartheta)=\sum_s I_s(H_s^\vartheta K_s^\vartheta L_i^\vartheta) \quad (2)$$

where $\sum_s$ is a summation by all points on the rods with indices $H_s^\theta K_s^\theta$ crossing the Ewald sphere at the scattering angle ϑ and corresponding to the *s*-components of *p* peak.

The result of such a procedure using a defined step in ϑ exhibits an intensity distribution which corresponds to broadening of the XRD peaks only due to the presence of stacking faults without taking into account crystal distortions and the finite crystallite size. The previous approach was used [16] to calculate the XRD peak profiles in the case of *fcc* crystal containing different planar defects. As a consequence, it was established that different types of defects affected variously the XRD peak profiles, and the parameters characterizing the XRD peak position and profile are dependent on the defect concentration in a non-monotone way. These results are evidence when a quantitative investigation of the microstructure of the crystal containing planar defects has to be based on a full-profile fitting of the experimental XRD diagrams.

$S_s(\vartheta)$ is the function describing the *s*-component broadening due to the finite size of crystallites; according to [6], the XRD peak profile can be fitted by a superposition of Lorentzian and Gaussian functions for which the integral breadth, B_s at the angle ϑ is defined by Scherrer's equation: $B_s = \lambda/(D\cos\theta)$, where λ is the wavelength of the X-ray radiation and D is the mean size of the coherently diffracting domains.

$D(\vartheta)$ is the function describing XRD peak broadening due to the microdistortions of the crystal lattice; from results reported by Ungar *et al.* [24], the integral breadth, B_d, of the XRD peak at the angle ϑ can be presented, on a first approximation, as $B_d = 2E\rho^{1/2}C_{hkl}\mathrm{tg}\,\vartheta$, where $E = \rho^{1/2}(\pi A^2 \boldsymbol{b}^2/2)^{1/2}$, A is a parameter which depends on the effective outer cutoff radius of dislocations, $\boldsymbol{b}$ is the Burgers vector, C_{hkl} is the mean factor of the dislocation contrast of the *hkl* peak, ρ is the dislocation density.

$A(\vartheta)$ describes the XRD peak broadening caused by the instrumental factors. Summation should be performed for all components of a peak.

EXPERIMENTAL VALIDATION

An analysis of the experimental XRD diagrams and subsequent fitting of the diagrams were performed according to the procedure discussed above. The Gauss and Lorentz functions with integrated breadths, respectively, B_s and B_d were used as the functions describing the size factor and distortion factor, respectively. The best agreement between the experimental and the calculated XRD peak profiles for different *hkl* indices was achieved by the variation of the parameters α, D and ρ at the condition of both the size factor and microdistortion factor are the Lorentz functions.

As an illustration, the peak profile of experimental XRD diagram for different copper

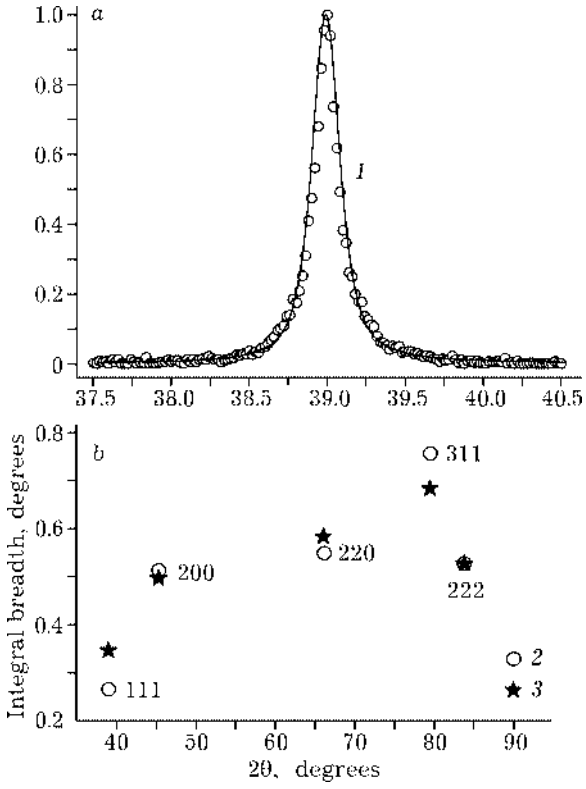

Fig. 4. Comparison between: *a* – the experimental XRD peak (111) and calculated XRD peak (*1*), *b* – the experimental peak breadths (*2*) obtained in the case of the ball milling condition 250/50/24 h and those obtained from the simulated powder X-ray diagram (*3*).

powders is shown in Fig. 4 with the corresponding peak profile modelled by the proposed approach. One can see that a satisfactory agreement is observed between the measured and modelled XRD peak profiles in the case of initial Cu powder and milled Cu powders prepared under different ball milling conditions. Results of the experimental data processing according to the procedure described above are shown in Table 2.

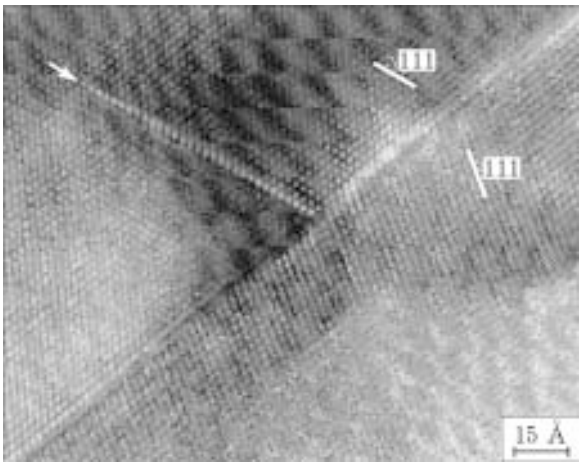

Fig. 5. HRTEM observation of nanopowders.

One can notice:

– that the non-monotonous character of the dependence of the integral breadth with respect to the scattering angle is satisfactorily described by the proposed model.

– the XRD data indicate that the positions of XRD peaks correspond to their Bragg positions with a high degree of accuracy. Moreover, experimental XRD peak profiles are symmetric. In concordance with the modelling results, these features evidence that powder contains neither intrinsic nor extrinsic faults [15], and the twin faults are the most likely present in the structure of the materials.

– HRTEM observations were performed. For example, a high-resolution image of a Cu-nanograin (diameter 35 nm) is presented in Fig. 5. The centre of the particle is metallic copper oriented with a <110> zone axis parallel to the electron beam. The linear contrasts crossing the particle are associated to {111} twin boundaries. These twin planes are also observed

TABLE 2

Microstructural characteristics of the Cu powders produced by ball milling

Ω (r.p.m.)/ω (r.p.m.)/Δ*t* (h)	Results of the fitting			Results of Williamson–Hall method	
	Concentration of the twin SF, γ, %	Mean size of crystallites, *D*, nm	Dislocation density, ρ, 10^{12} m^{-2}	Mean size of crystallites, *D*, nm	Microdistortions, %
0/0/0	0.3	120.6	0.46	121.7	0.07
150/50/24	0.87	73.8	1.9	41.3	0.16
250/50/24	1.51	47.2	6.3	24.9	0.25
350/50/24	1.88	31.2	14.1	20.7	0.41

in grains of copper nanopowder synthesised by the cryomelting process [18]. Moreover, Huang *et al.* [19] reported that multiple twins and high-order twins are also frequently observed in grains of copper nanopowder milled for 20 h. From these different observations, the presence of twin faults was taken into account in the modelling.

– the mean value of the crystallite size obtained by the XRD peak profiles fitting is nearly equal to the value determined from the Williamson–Hall method in the case when the SF concentration is low, as is shown in Table 2, in which the results from both procedures (our and Williamson–Hall) are presented. Indeed, an increase in the twin SF concentration leads to an increase in the crystallite size difference determined by these two methods.

Such changes of the Cu microstructure parameters are in agreement with those expected when the materials are subjected to mechanical treatment.

CONCLUSION

Analysis of the XRD powder patterns calculated in the case of a *fcc* polycrystalline metal structure, containing a high concentration of planar defects, shows that shapes and positions of the XRD peaks are qualitatively dependent on the type of stacking faults. The established features of transformation of the XRD peak profiles, as the concentration of the stacking faults increases, can be used to reduce a number of parameters used in the fitting process. On the basis of the developed approach, a successful fitting of the experimental data was performed by the simulation of XRD patterns of *fcc* crystals getting stacking faults, and taking into account the finite size of crystallites and microdistortions caused by the presence of dislocations. However, more information concerning the microstructure of these materials should be obtained, for example, by means of the transmission and/or secondary electron microscopy (TEM, SEM) in order to optimise the fitting procedure. This optimisation concerns, on the one hand, the reduction of the number of varied parameters by identification of stacking fault types and, on the other hand, the improvement of the calculation accuracy taking into account, for example, the known shape of the crystallites or their distributions.

REFERENCES

1 A. I. Ustinov, Defect and Microstructure Analysis by Diffraction, in R. L. Snyder, J. Fiala and H. J. Bunge (Eds.), Oxford University Press, 1999, p. 264.
2 B. E. Warren, X-Ray Diffraction, Massachusetts Addison-Wesley, 1969, p. 275.
3 A. J. C. Wilson, X-Ray Optics, 2nd Ed., London Methuen, 1962.
4 A. Revesz, T. Ungar, A. Bordely, J. Lendvai, *Nanostructured Mater.*, 7, 7 (1996) 779.
5 H. H. Tian, M. Atzmon, *Phil. Mag. A*, 79, 8 (1999) 1769.
6 T. Ungar, S. Ott, P. G. Sanders *et al.*, *Acta Mater.*, 46, 10 (1998) 3693.
7 L. Velterop, R. Delhez, Th. H. De Keijser *et al.*, *J. Appl. Cryst.*, 33 (2000) 296.
8 P. Scardi, M. Leoni, *Ibid.*, 32 (1999) 671.
9 G. K. Williamson, W. H. Hall, *Acta Metall.*, 1 (1953) 22.
10 B. E. Warren, B. L. Averbach, *J. Appl. Phys.*, 23 (1952) 497.
11 E. Gaffet, M. Abdellaoui, N. Malhouroux-Gaffet, *Mater. Trans. JIM*, 36 (1995) 198.
12 M. Abdellaoui, E. Gaffet, *Acta Mater.*, 44, 2 (1996) 725.
13 E. Gaffet, L. Yousfi, *Mater. Sci. Forum*, 88–90 (1992) 51.
14 J. I. Langford, D. Louer, *Rep. Prog. Phys.*, 59, 2 (1996) 131.
15 A. I. Ustinov, L. A. Olikhovska, N. A. Budarina, F. Bernard, Diffraction Analysis of the Microstructure of Materials, in E. Mittemeijer and P. Scardi (Eds.), Springer, Berlin, 2003 p. 333.
16 A. I. Ustinov, N. M. Budarina, *Powder Diffraction*, 17 (2002) 7.
17 B. E. Warren, *Prog. Met. Phys.*, 8 (1959) 147.
18 Y. Champion, J. Bigot, *Scripta Mater.*, 35 (1996) 517.
19 J. Y. Huang, Y. K. Wu and H. Q. Ye, *Acta Mater.*, 44, 3 (1996) 1211.